Cellulose (2023) 30:9669–9691
https://doi.org/10.1007/s10570-023-05467-3

ORIGINAL RESEARCH

Cellulose-based hydrogel beads derived from wastepapers: application for organic dye adsorption

Mohammad Rezvani Ghalhari · Daryoush Sanaei · Ramin Nabizadeh · Amir Hossein Mahvi

Received: 10 September 2022 / Accepted: 20 August 2023 / Published online: 13 September 2023

Abstract Some adsorbent hydrogels made of natural polymeric materials have not yet met the needs for a high level of wastewater purification. In the present study, a novel and environmentally friendly process is described for the production of natural cellulose-based metal oxide nanoparticle hydrogel beads. Recyclable adsorbent components include wastepaper-derived cellulose fiber, metal oxide nanoparticles and polyvinyl alcohol was synthesized, the WCF/PVA MO NP hydrogel beads were synthesized by using cross-linking agents (Ca^{2+}, boric acid and NaCl), and were analyzed by evaluating their ability to remove the acid red 18 (AR18) from aqueous solution. The WCF/PVA MO NP was characterized by FESEM, XRD, EDX, BET, and FTIR. The results revealed that the metal oxide nanoparticles distributed on external and internal channels of the 3D fiber network of WCF with strongly covalent/non-covalent cross-linking bonds would facilitate mass diffusion and enhance the interaction between AR18. The results shown that more than 87.62% of AR18 was removed and adsorption capacity was 88.65 $mg{\cdot}g^{-1}$ under optimized conditions ([AR18]: 10 $mg{\cdot}L^{-1}$; [adsorbent]: 0.55 $g{\cdot}L^{-1}$; pH: 3; Time: 46 min). Results shown that the adsorption kinetics fit the pseudo-second-order model (0.99), and the adsorption isotherms fitted to Langmuir isotherm model (0.99).

Supplementary Information The online version contains supplementary material available at https://doi.org/10.1007/s10570-023-05467-3.

M. R. Ghalhari · R. Nabizadeh · A. H. Mahvi (✉)
Department of Environmental Health Engineering, School of Public Health, Tehran University of Medical Sciences, Floor Number 5, Ghods Avenue, Enghelab Street, Enghelab Square, Tehran, P.O. Box 14155-6446, Iran
e-mail: Ahmahvi@yahoo.com

M. R. Ghalhari
Student's Scientific Research Center, Tehran University of Medical Sciences, Tehran, Iran

D. Sanaei
Department of Environmental Health Engineering, Faculty of Public Health and Safety, Shahid Beheshti University of Medical Sciences, Tehran, Iran

R. Nabizadeh
Center for Air Pollution Research (CAPR), Institute for Environmental Research (IER), Tehran University of Medical Sciences, Tehran, Iran

Graphical abstract

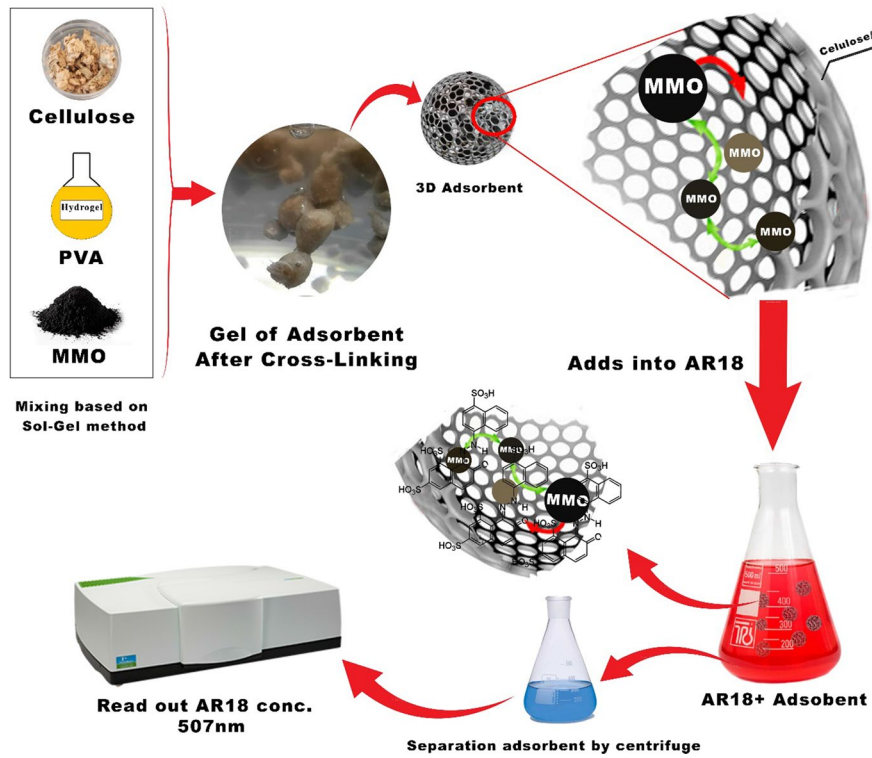

Keywords Wastepaper-derived cellulose fibers · Sacrificial cross-linking · Hydrogel beads

Introduction

Hydrogels are considered an effective material that is applicable in different applications which are ongoing interest for scientists working in water purification (Araki 2021). Hydrogels exhibited a desirable, porous polymeric network with many interior and exterior channels and surfaces held together by either physical or chemical cross-linking (Li et al. 2022b). There are multifarious hydrophilic functional groups such as carbonyl, hydroxyl, etc. (Li et al. 2022a). They have been a popular topic when developing novel adsorbents that are able to remove pollutant from aqueous solution rapidly; these hydrogels can successfully be prepared from various sources (Abe and Yano 2011; Mondal et al. 2022).

Among the biopolymers, cellulose is the most multitudinous material on the earth, therefore, having promising potential in the preparation of hydrogel (Alizadeh-Sani et al. 2021; Jiang et al. 2022). Cellulose consists of a chain of β-(1 → 4)-linked D-glucose units that featured strong mechanical or chemical properties (Siripongpreda et al. 2021). With its abundant functional groups in their backbone and hydrophilic characteristics, cellulose would be considered a promising adsorbent hydrogel for purifying aqueous solutions from organic pollutants (Lyu et al. 2021). There is abundant biological/chemical/biomass, and waste sources as the precursor for the fabrication of cellulose (Joshi et al. 2015; Xie et al. 2021).

The capability of cellulose for water reabsorbing and retention capacity as the hydrogel and adsorbent material are limitations (Chen et al. 2017). Here, to overcome these problems, the WCF blended with Polyvinyl Alcohol (PVA) to form hydrogel beads to improve their chemical and physical stabilities (Dai et al. 2018). Hence, in this study, incorporating

metal oxide nanoparticles into WCF/PVA hydrogel beads (WCF/PVA MO NP hydrogel beads) could be added as additional active metal–acid sites to relieve consumed functional groups, which can be carried out to remove the pollutants such as dyes from aqueous solutions (Alibak et al. 2022; Kumar et al. 2013). Recent studies play a role about adsorption process progress and cellulose compounds such as carboxymethyl cellulose, which are environmental compound can be used as a suitable hydrogel to remove dyes from wastewater (Chen et al. 2019; Lin et al. 2017; Wang et al. 2021, 2022) also, in the recent research a cellulosic adsorbent named a super adsorbent which have a acceptable ability in macromolecules pollutants (Peng et al. 2016).

Organic dyes are used in various industries such as the textile (Beh et al. 2020; Sillanpää et al. 2021), solvent industry, foods, drugs, plastic, inks, varnishes, paints, paper, wood, leather, rubber, and cosmetics (Dalvand et al. 2016; Mirzadeh et al. 2014; Wang et al. 2020). Synthetic dyes such as Acid Red 18 (AR18) are usually considered not biodegradable due to their complex aromatic structures, making them stable to light, heat, and oxidizing agents (Hamidi et al. 2022). In recent years, diverse biological and physicochemical approaches have been used to remove the dyes from aqueous solutions (Azari et al. 2020; Bazrafshan et al. 2016, 2013; Gholami-Borujeni et al. 2011a, b).

Adsorption is one of the most significant and cost–benefit approaches for removing dyes such as AR18, which is widely distributed in the environment and soluble in aquatic solutions (Shirmardi et al. 2012). Meanwhile, biologically based adsorbents are acceptable because they do not add secondary pollution to the environment (Ashrafi et al. 2013; Hashemkhani et al. 2022; Sani et al. 2022). However, the preparation of cellulose from some resources is not cost-effective. The cellulose fibers can be extracted effectively from wastepaper as a raw carbon source with a simple and cost-effective method (Kord Mostafapour et al. 2022; Shadkam et al. 2021). Therefore, this research study aimed for sustainable production of cellulose-based hydrogel beads by recycling wastepaper utilizing sacrificial cross-linking agents for efficient removal of AR18 from aqueous solution. In the present study, unlike other studies that have used a prepared and purchased cellulose, recycled cellulose from waste newspaper was used as the base of the green adsorbent.

Materials and methods

Sample analysis and chemicals

All chemicals which were used in this work were of analytical reagent grade (AR) and did not have any further purification. In this study, Double distilled water (Milli-Q Millipore 18.2 MΩ cm^{-1} conductivity) was used for the preparation of a stock solution of The AR18 dye (molecular formula, $C_{20}H_{11}N_2Na_3O_{10}S_3$, MW: 604.4766 g/mol, assay: ~ 99%, $\lambda_{max} = 507$ nm) which was purchased from Sigma-Aldrich (NEW COCCINE C.I. 16255) of 1000 mg/L concentration and other solution. Stock solutions of AR18 were prepared by dissolving 1 g of AR18 in 1L Double distilled water without any pH adjustment. We collected newspapers from one commercial office. The other reagents utilized throughout this study were analytical grade. A portable pH meter (Kent EIL, 7020) Model was used to measure pH values in the aqueous phase. Batch equilibrium adsorption experiments were performed using 50 mL of the AR18 solution. After the adsorption process, the adsorbent was separated from the samples by centrifugation (5000 rpm and 15 min) (LC-8 Lab Centrifuge). Finally, the filtrate samples were analyzed by UV–vis spectrophotometer (Perkin Elmer Lambda 25) at 507 nm (Heibati et al. 2015a). The pH of WCF/PVA MO NP hydrogel beads at the point of zero charges (pHpzc) was determined based on the literature using NaCl 1 M (Dalvand et al. 2016). Also, because NaOH in the presence of CO_2 can be changed to Na_2CO_3, to prevent Na_2CO_3 intervention in the results, 0.8 M $Ba(OH)_2$ was added to NaOH solution (Edzwald and Association 2011).

Synthesis

Wastepaper derived cellulose fibers (WCF) extraction

A paper shredder (Kores 827) was used to cut waste newspapers into small pieces (1 mm × 1 mm). To remove the ink, oil, and dye in the paper; NaOH 5% by weight and sodium bicarbonate 3% by weight was used at 80–65 °C in two stages separately. A Whatman 40 filter and double-distilled water (5 times)

were used for the first rinse. In the next step, to remove the remaining paint and oil fixed on cellulose fibers, 200 ml of sodium bicarbonate 3% was added to the doughy solution and placed on the magnetic stirrer for 2.5 h at 50–80 °C. For the second rinse, the final cellulose fibers were rinsed well (8 times) with double distilled water until pH adjusted between 7 and 7.5. Finally, to remove any moisture on cellulosic fiber, an oven was carried out (MEMERT) at 180 °C for 3 h. Then the dried cellulosic fiber was transferred to a desiccator (Dehghani et al. 2016).

Metal oxide nanoparticles (MO NP) synthesis

To increase the adsorption capacity, several metal nitrate salts were used, including Fe $(NO_3)_3{\cdot}9H_2O$, Co $(NO_3)_2{\cdot}6H_2O$, Mn $(NO_3)_2{\cdot}4H_2O$, and Sr $(NO_3)_2$. For the first, in the separate 25 mL volumetric flasks, 0.5 M, 0.5 M, 0.3 M, and 0.7 M of Co $(NO_3)_2{\cdot}6H_2O$, Fe $(NO_3)_3{\cdot}9H2O$, Mn $(NO_3)_2{\cdot}4H_2O$ and Sr $(NO_3)_2$, respectively were prepared, and these solutions were mixed for 10 min (100 rpm). Then, 0.66 M EDTA ($C_{10}H_{16}N_2O_8$) and 1.89 M citric acid ($C_6H_8O_7H_2O$) were prepared separately in 25 mL volumetric flasks and mixed with metals solutions with molar ratios of 1/1.3/1, respectively. Then, by adding ammonia 25%, the solution's pH was adjusted to 6. Then, a prepared solution based on a sol–gel method should be placed on a magnetic stirrer at 95 °C for 3 h until a gel-like substance is observed. The gel-like substance of MO NP is transferred to an oven 450 °C for 8 h (the specific flow hot rate was 5 °C·min^{-1}) to create a solid-like substance. After this step, the solid formed should be put at ambient temperature for 10 min, transferred back to the oven, and again set the oven temperature at 800 °C for 6 h (specific flow hot rate was 5 °C·min^{-1}). Finally, the product dried at ambient temperature.

WCF/PVA MO NP hydrogel beads preparation

To prepare the hydrogel beads, 100 mL of Polyvinyl alcohol (PVA) solution (7% w/w) was magnetically stirred at 75 °C for 8 h. Then, WCF (2 g) was added to the PVA solution and stirring continued for 45 min (the ratio of WCF/PVA by considering weight was $\frac{2}{7}$). After cooling the WCF/PVA solution to room temperature, MO NP powder (0.3 g) was added to the WCF/PVA solution and magnetically stirred for 4 h.

To establish a connection between the solution's various components, WCF/PVA MO NP Hydrogel Beads solution was injected into the linking solution. The linking solution included 50 mL calcium chloride (5% w/w)50 mL sodium chloride (0.5% w/w), and 50 mL saturated boric acid at pH 4. To inject WCF/PVA MO NP Hydrogel Beads solution, a peristaltic pump with a fixed flow rate (15 mL/h) was used (the distance between the surface of the linking solution and peristaltic pump should be adjusted on 12 cm). After several hours, the beads-like shapes created in the linking solution were kept for 60 h. Then, to remove the linking solution from the adsorbent beads, the adsorbent was rinsed several times with doubled distilled water and passed through Whatman paper 0.45 µm. Finally, the prepared hydrogel beads were kept at freezer − 55 °C on the freezer (CARLO ERBA, ULT-388) and pressure adjusted on 3.5 Pascal; after 36 h, WCF/PVA MO NP Hydrogel Beads were ready for our experiments in dye removal. The general schematic of the synthesis process is shown in Graphical Abstract.

Characterization of WCF/PVA MO NP hydrogel beads

Instrumental analysis

Surface characteristics and morphology of the WCF/PVA MO NP hydrogel beads were investigated by scanning electron microscopy (SEM, MIRA3-XMU) before and after AR18 dye adsorption. Adsorbents were coated via gold then accelerating voltage of 20 kV was used to observe. Also, to detect the spatial distribution of various elements in the adsorbents, for this purpose element mapping (MAP) was performed by a wavelength dispersive X-ray spectroscopy (WDS) method. To identify the functional groups of WCF/PVA MO NP hydrogel beads before and after AR18 dye adsorption, Fourier Transform Infrared (FTIR) spectrometer (Perkin-Elmer, Spectrum RX I) was used. This study determined the crystallographic structure of WCF/PVA MO NP hydrogel beads by using X-ray diffraction analysis (XRD) (XRD Philips PW1730), it should be noted that a nickel-filtered Cu Kα at wavelength of 0.154 nm radiation beam in the range 4 to 77° 2θ for 2 h by considering scanning rate of 0.5°/min at room temperature at a voltage of 45 kV and the current of 20 mA were used to record

the XRD spectra. To carry out surface area analysis, we used Brunauer–Emmett–Teller (BET), which was performed on a PMIs' Automated BET Sorptometer (SSA-4300, Beijing Builder, Inc., Beijing, China). For this analysis, neutral gases should be used in the tests of this analysis.

Batch adsorption experiments

All adsorption experiments were carried out in a batch manner to study the effect of parameters including pH (2–10), adsorbent dosage (0.1–1 g L^{-1}), initial AR18 concentration (10–250 mg L^{-1}), and contact time (0–90 min) on adsorption of AR18 onto WCF/PVA MO NP hydrogel beads. All experiments were performed at 150 rpm on a shaker (Lab Companion SK-300 Benchtop Shaker). The AR18 stock solution was prepared with a concentration of 1000 mg L^{-1}; 1 g of AR18 powder dissolved in distilled water.

To adjust the solution's pH, sodium hydroxide (NaOH) 0.1 N and hydrochloric acids (HCl) 0.1 N were used. All the experiments were carried out in triplicate. The concentration of AR18, which adsorbed per unit mass of the WCF/PVA MO NP hydrogel beads (q_e) was calculated by using the following mass balance equation (Eq. 1), and the removal efficiency was calculated by using the following Eq. (2):

$$q_e = \frac{(C_i - C_e)V}{w} \quad (1)$$

$$\text{Removal efficiency } (\%) = \frac{(C_i - C_e)}{C_i} \times 100 \quad (2)$$

where C_i is the initial concentration of AR18 and C_e is residual concentrations of AR18.

Experimental design, data analysis, and process optimization

This study used response surface methodology-based central composite design (RSM-CCD) to model and optimize the AR18 adsorption process by WCF/PVA MO NP hydrogel beads. The experimental central composite design (CCD) matrix, with the not codified values for all factors presented in Table S1 (See Supplementary materials).

Statistical significance of the fitted quadratic models, influential factors, and their interactions on response was also analyzed using analysis of variance (ANOVA) tests ($P < 0.05$), R^2, and linear regression model. The experiments were designed and analyzed by R software, version 3.6.0 (Missouri, USA), and OriginPro 2017 software. Before determining each parameter's full effect, a full factor study (effect study) was carried out and analyzed with linear regression.

Results and discussion

Characterization of WCF/PVA MO NP hydrogel beads

FE-SEM/EDX-mapping

The cellulose fiber extracted from wastepaper as an ideal host to distribute metal oxide particles using PVA as a stabilizer to control the growth of nanoparticles for reducing aggregations and deactivation were demonstrated by performing FE-SEM images (Fig. 1a and Supplementary Fig. 1). The wastepaper-derived cellulose fibers (WCF) exhibited a lot of networks of fibers with various size from 25 to 60 nm (the size of fiber's networks determined by ImageJ program (Abràmoff et al. 2004)). Moreover, most WCFs have depicted a fiber length from a few mm to even longer. The metal oxide nanoparticles gradually developed and distributed on external and internal channels of the 3D fiber network without significant aggregation (Fig. 1b). The –OH surface groups of WCF/MO NP hydrogel beads composite as nucleation sites for metal oxide NPs, the cross-linking reaction between the surface of composite and cross-linking reagent during the beads-like composite process, and there is intermolecular H– bonding in crystalline areas of WCF networks could be considered as main reasons for uniformly distributed and non-agglomerated MO NP on extracted cellulose fibers. It is important to note that the distributed MO NP on WCFs are presented as white dots (Fig. 1c and d). Moreover, it can be seen that the MO NP remained well intercalated and distributed on the fiber and layer structure of WCF/MO NP hydrogel beads after the AR 18 adsorption process (Fig. 1e and Supplementary Fig. 1). The 3D interconnected network and mainly micro-porous

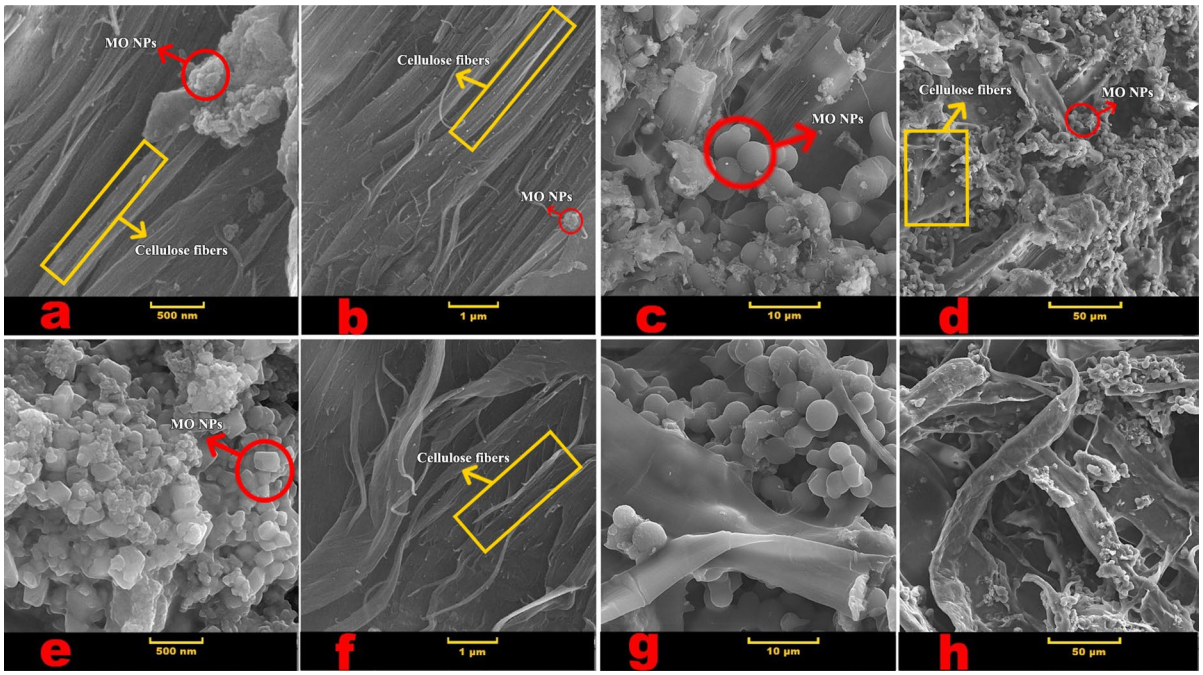

Fig. 1 SEM images of pure WCF/PVA MO NP hydrogel beads (**a**, **b**, **c**, **d**) and WCF/PVA MO NP hydrogel beads after adsorption of AR18 dye (**e**, **f**, **g**, **h**)

structure on the interior channel networks of WCF/MO NP hydrogel beads would improve the opportunity of interaction between the AR 18 and the Interface of WCF/MO NP hydrogel beads, hence, empowering its adsorption capacity (Fig. 1f, g and h). Generally, the MO NP that exists in the WCF/MO NP hydrogel has a specific and orderly pore size distribution and is placed on the long cellulose fibers, which makes them a suitable site for AR 18 molecule adsorption.

The distribution and quantity of elementals in WCF/MO NP hydrogel beads were further carried out by using EDX-mapping analysis (Fig. 2). Moreover, the percentage of elements in WCF/MO NP hydrogel beads from the EDX technique are provided in the Tables inserted in Fig. 2c, d. The carbon content from WCF and PVA is successfully extracted as 55.9% w.t of WCF/MO NP hydrogel beads. Interestingly, the higher oxygen of content that is beneficial for adsorption process is provided from the distribution of metal oxide NPs onto WCF. The content of metal oxide was in agreement with the synthesis phase. Furthermore, the EDX—mapping analysis was carried out for WCF/MO NP hydrogel beads after adsorption of AR 18. As can be seen from the Tables Inserted in Fig. 2c, d, after the adsorption process, the content of all elements (except carbon) was slightly increased to some extent, corresponding to the ion exchange in the adsorbate solution through the adsorption process. It is important to note that after the AR 18 adsorption process, Fig. 2a shows that the adsorbent was relatively stable, and its morphologies were slightly affected by the adsorption. After adsorption, the pores of WCF/MO NP hydrogel beads are covered by a thin layer of dye that also agrees with observed morphology changes after dye adsorption (Re).

FT-IR analysis

The FT-IR spectra of WCF/PVA MO NP hydrogel beads before and after the adsorption of red dye acid 18 are shown in Fig. 3a. Identification of factor groups in the composition was performed by FT-IR spectrum. The vibration peak is about 3300 cm^{-1}, representing O–H stretching vibration (Maiti et al. 2020). The peak of about 2872 cm^{-1} is related to the aliphatic CH stretching vibrations, and 1424 cm^{-1} may be related to C–H bending

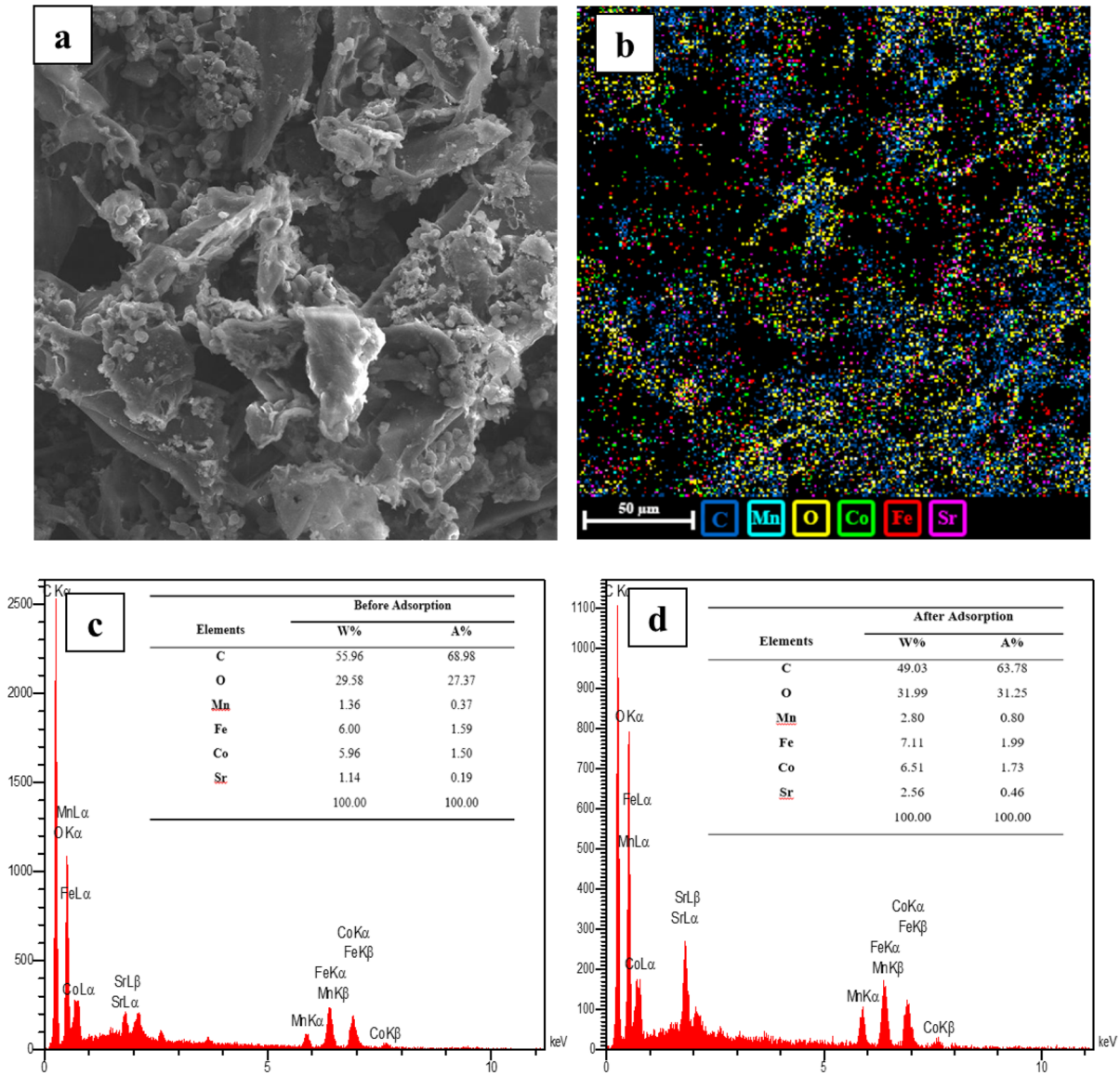

Fig. 2 Low magnification FE-SEM image (**a**), EDX elemental maps of WCF/PVA MO NP hydrogel beads (**b**), corresponding EDX spectrum of WCF/PVA MO NP hydrogel beads before adsorption of AR18 (**c**), and corresponding EDX spectrum of WCF/PVA MO NP hydrogel beads after adsorption of AR18 (**d**)

vibrations (Thombare et al. 2023; Wang et al. 2019). The stretching C–O peak is formed in 1300 to 1000 cm^{-1}. Therefore, the peaks in 1034 cm^{-1} and 1149 cm^{-1} are related to the stretching vibration of C–O, C–O–C, and C–OH of ether and alcohol groups, respectively. The peak of 1630 cm^{-1} is also related to the O–H molecule of water absorbed by cellulose (Atykyan et al. 2020; Jin et al. 2015). In the FTIR spectrum of the samples after AR18 adsorption, in addition to the cellulose-related peaks mentioned above, a bending vibration of NH related to the structure of red acid 18 is observed at 1531 cm^{-1}, which indicates the adsorption of dye by WCF/PVA MO NP hydrogel beads (Jin et al. 2015).

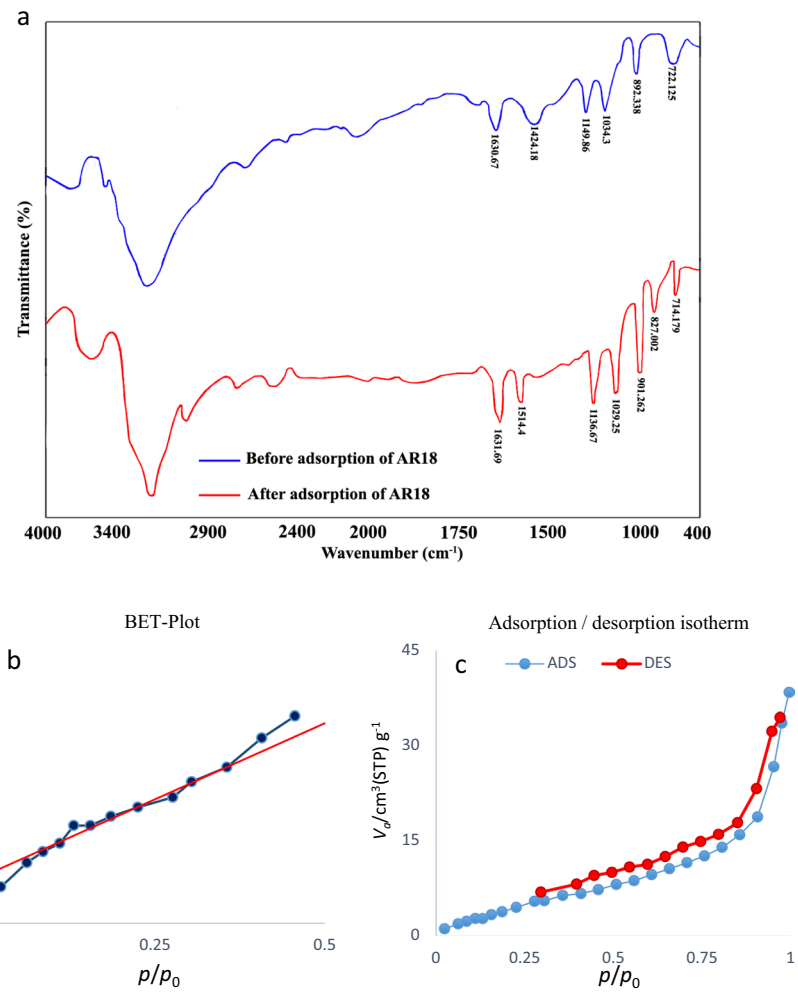

Fig. 3 FTIR analysis of WCF/PVA MO NP hydrogel beads before and after AR18 adsorption (**a**) BET analysis (**b**) adsorption/desorption analysis (**c**)

BET test

The adsorption mechanism in the first stage is a monolayer. It then changes to multilayer due to the non-uniformity of the adsorbent surface and the interaction of gas molecules with each other. The adsorbent surface was confirmed according to performed BET analysis. The BET adsorption theory was proposed for multilayer adsorption conditions to correct the flaws of the Langmuir theory (Ebadi et al. 2009). The results of the BET test in Fig. 3b show that WCF/MO NP hydrogel beads possessed a high specific surface area (22.536 m^2/g) and pore volume (0.053 m^3/g), indicating its porous structure in SEM and uniformly distribution of MO NP and strong cross-linking on the WCF support. Moreover, based on the International Union of Pure and Applied Chemistry (IUPAC) (Sotomayor et al. 2018), type IV adsorption–desorption isotherms with hysteresis are achieved by WCF/MO NP hydrogel beads (Fig. 3c), reflecting the presence of both micropore (~ 1.85 nm) and mesopores (~ 3.52, and 6.94 nm). Interestingly, the co-existence both of micropores and mesopores would provide adequate space for the mass transport of dye molecules and high accessibility of active sites for dye molecules that reside in micropore structures. If the P/P^0 ratio is low, it is similar to the type IV isotherm. But, when this ratio is very large, the material has very narrow capillary pores, which increases the adsorption rate significantly. The obtained result suggests that the co-intercalation of PVA/WCF and cross-linking agents in WCF/MO NP hydrogel beads regulated

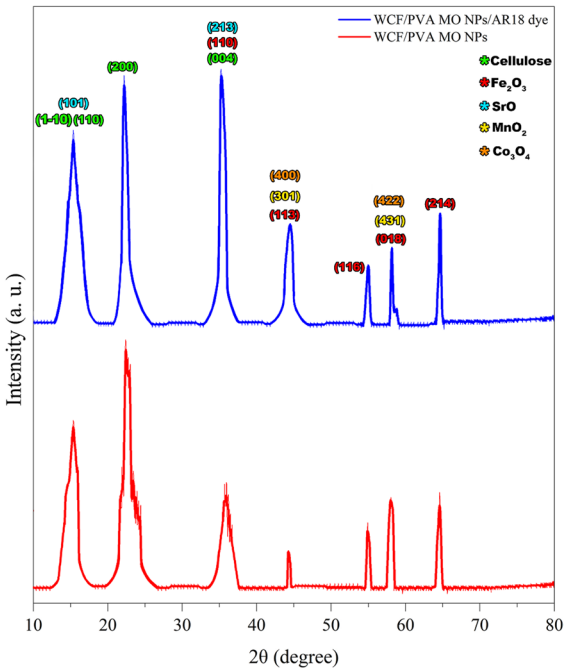

Fig. 4 XRD patterns of WF/PVA MO NP hydrogel beads before and after AR18 adsorption

the interconnect pore structures and accessibility of active site of the as-synthesized hydrogel beads.

XRD patterns

The X-ray diffraction analysis was conducted to investigate the crystallographic structure of WCF/PVA hydrogel beads containing MO NP (Fig. 4). A broad range of diffraction peaks was revealed at 2θ = 15.32, 19.57, 22.59, 26.45, 27.28, 30.20, 35.92, 38.61, 54.91, 57.51, 60.31, 63.02, 70. 62 and 74.3° which confirmed the crystal plane of Fe_2O_3 and Co_3O_4 NPs in the composite MO NP structure (see Table S2). The diffraction peaks appearing at 2θ = 27.82° and 2θ = 19.57 and 26.45° are exclusively related to Fe_2O_3 and Co_3O_4, respectively. Likewise, the diffraction peaks related to MnO_2 and SrO appeared at 2θ = 35.55, 40.04, 43.36, 51.92, 57.35, 60.61, 62.81, 70.35, 71.37, and 75.74° and 2θ = 32.85, 38.7, 46.95, and 58.4°, respectively. All resulting diffraction peaks agree with the reported patterns including Joint Committee on Powder Diffraction Standard (JCPDS): 039-1346 (Fe_2O_3), JCPDS: 073-1701 (Co_3O_4), JCPDS 44-0141(MnO_2) and JCPDS 00-006-0520 (SrO), indicating high purity of the crystal system (Athar 2013; Chaugule et al. 2019; Wang et al. 2014; Wu et al. 2011). WCF/PVA MO NP hydrogel beads showed nearly the similar XRD pattern before and after adsorption of AR18 dye. As provided in the Table S2, for the composite metal oxide nanoparticles consisting of MnO_2, Fe_2O_3, Co_3O_4 and SrO compounds, the XRD peaks corresponded to their expected confirmed values by the Expert program demonstrating the obvious crystallinity of metal oxide species. Miller indices of (1-10), (110), and (200), which were also employed in the French (2014) study, are the primary intensity contributors to the three major peaks (French 2014).

The formation principle of the prepared hydrogel beads

The prepared hydrogel was first made by distributing MO NP into wastepaper-derived cellulose fibers (WCF) by means of one-step mixing with PVA as a cross-linker and then slowly dripping the mixed solution into the bath of cross-linking agents. As well known, PVA is a hydrophilic polymer that is expectantly applied as cross-linking between the WCF and PVA due to plentiful hydroxyl groups producing inter and intra-chain Hydrogen bonding and van der Waals forces. Figure 5a presented the repeating unit of cellulose (French 2017), As shown in Fig. 5a, the cross-linking occurs between OH groups in PVA and the carboxymethyl or dicarboxylic groups on WCF as a result of H-bonding. However, PVA's hydrophilicity reduces mechanical properties because of high water absorption, restricting its applicability as an adsorbent or catalyst. The modification of cross-linking the PVA chains could be reduced water absorption. Hence, In the second step, the mixture of WCF-MO NP-PVA is immersed in cross-linking solutions, including calcium chloride ($CaCl_2$), NaCl, and oversaturated H_3BO_3. The H_3BO_4 is hydrolyzed to yield a Borate ion that then reacts with PVA and WCF. Due to the existence of free hydroxyl groups in PVA and WCF, it is expected that the cross-linking reaction of borate ion with PVA and WCF would happen; the cross-linking mechanisms are shown in Fig. 5b. The ascribed peaks at 1424 cm^{-1} and 1149 cm^{-1} assigning to the bonds B–O and B–O–C respectively (Fig. 3a). Moreover, boron atom containing empty p orbitals are considered as electrophilic that could be attract

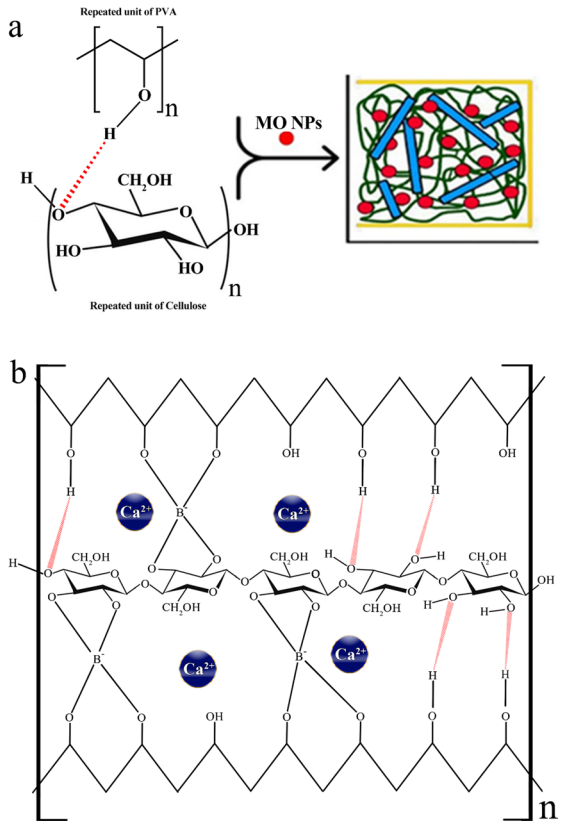

Fig. 5 The formation principle of the WCF/MO NP hybrid beads

nucleophilic hydroxyl groups of WCF/PVA, suggesting the formation of cross-links. Moreover, the physicochemical interaction of Ca^{2+} with the carboxylate groups exist in the hydrogel beads could be created an additional cross-linking point. Hence, as well known, the cross-linking plays a significant role in the formation and enhancement of the properties of superabsorbent hydrogel beads. Due to various cross-linking and unequal reaction speed rates between the surface of WCF/MO NP and PVA and mixture solutions, MO NP could be generated and distributed in hydrogel beads after adding metal precursors into the WCF-PVA solution. The PVA would slowly react with the $CaCl_2/H_3BO_3$ cross-linking liquid, and then plentiful nanostructures of fiber mesh were made on the inner and outer surface of hydrogel beads. Thus, a uniform distribution of MO NP displayed from nanoscale to submicron scale (Fig. 3c) on the outer and interior of surface hydrogel beads. The multi-porous structures and distribution of MO NP on the WCF's interior and exterior channel surface would assist in increasing the opportunity of interactions between the cationic acid red 18 and the adsorbent-adsorbate interface. Hence, the adsorption capacity could be promoted and the recycling process could also be possible using these hydrogel beads.

Optimization of AR18 removal from aqueous solution using WCF/PVA MO NP hydrogel beads

Effect of pH on adsorption behavior The efficient adsorption process occurs when the ion structure converts to molecule structure; this is possible by the pH adjustment (Edzwald and Association 2011). The variation of the pH of the solution can result in a change in the surface charges of the adsorbent and the ionization degree of the solution adsorbate (Rahmani et al. 2018). As can be seen from Fig. 6c, d, and e, the amount of adsorbed capacity of WCF/PVA MO NP hydrogel beads was maximum at pH of 3 and then further decreased with increasing values of pH to 10. It can be safely assumed that this occurrence might be caused by the following two points (Edzwald and Association 2011). The protonation of the carbonyl and/or hydroxide groups at the surface of WCF/PVA MO NP hydrogel beads under an acidic situation could be responded to due to the attraction electrostatic between protonated functional groups and negative centers of the AR18. Moreover, the active sites of M (MO NP)-C of the adsorbent could be considered additional sites for adsorption of AR18.

On the one hand, the protonated process of the adsorbent surface is reduced as pH increases, corresponding to electrostatic repulsions between OH^- or carboxylate anions obtained from the ionization of the carboxyl groups and negative sites of dye molecules, which in turn retards the extent of diffusion and adsorption process thereby (Zhang et al. 2018). Moreover, the increased OH^- ions under alkaline pH could strongly compete with the anionic dye of molecules for the surface of hydrogel beads.

Effect of contact time on adsorption behavior One of the main parameters that can affect adsorption is contact time because contact time increases allows it to sift more molecules (Arora et al. 2019). The effect of contact time on AR18 removal was shown in Fig. 6a, b, and e. It was observed that the amount of removal of AR18 increases when contact time increases. After

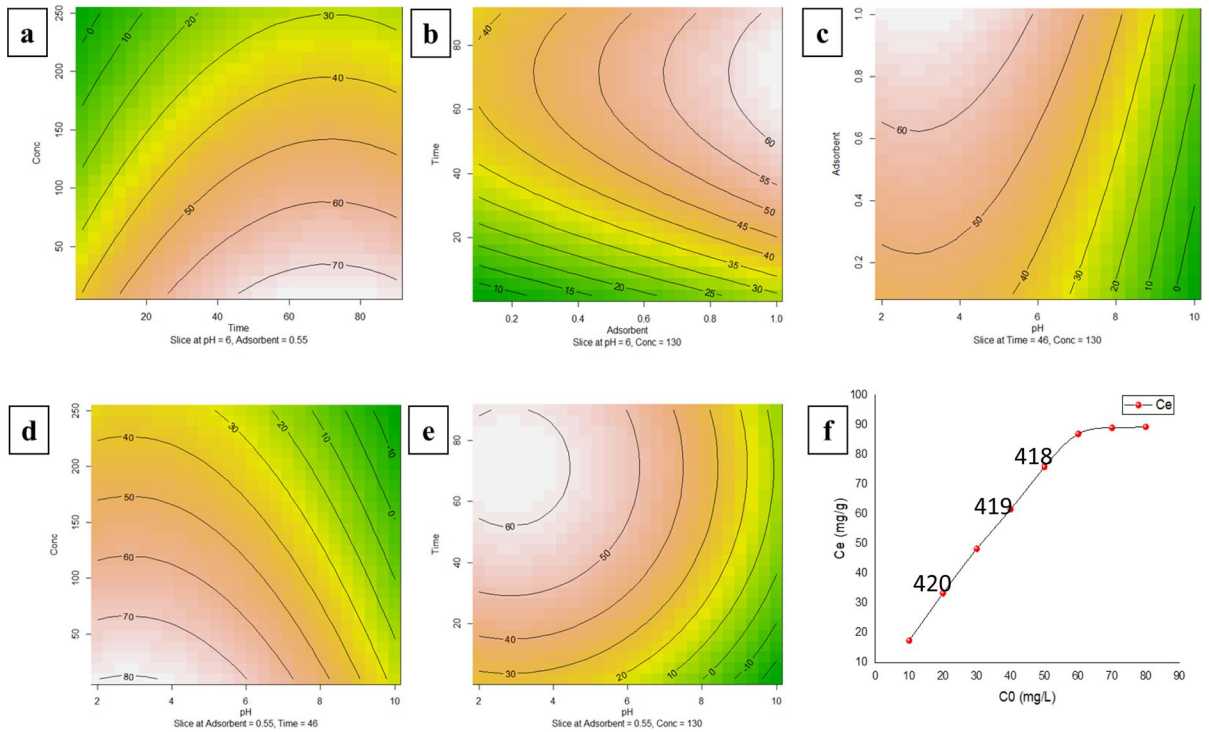

Fig. 6 Contour plots and main effect of variables (Contact time and AR18 concentration (**a**), Adsorbent and Contact time (**b**), pH and Adsorbent dose (**c**), pH and AR18 Concentration (**d**), pH and Contact time (**e**)) on AR18 removal (%) and **f** adsorption capacity of WCF/PVA MO NP hydrogel beads

several minutes AR18 is adsorbed quickly, and with time its adsorption process reaches equilibrium after 46 min. The AR18 adsorption equilibrium time was about 46 min by WCF/PVA MO NP hydrogel beads, removing 87.62% of the initial dye concentration at the WCF/PVA MO NP hydrogel beads surface for AR18 adsorption and over time, as more and more adsorbent sites are filled AR18 molecules.

Effect of adsorbent dosage on adsorption behavior Sorbent doses play a critical role in adsorption because more adsorbent dosages bring together pores and more sorption positions (Rejek et al. 2021). To determine the effect of WCF/PVA MO NP hydrogel beads dosage on adsorption, 0.1 to 1 g·L^{-1} were added to 10 mg·L^{-1} solution of AR18 dye. It was shown that removal of AR 18 increased from 87.62 to 95.3% with the increase in the amount of WCF/PVA MO NP hydrogel beads from 0.1 to 1 g·L^{-1}, because by increasing adsorbent dosage, the porous sites increase so more dye molecules were adsorbed. (Fig. 6b and c). Adsorption capacity depends on the presence of vacant sites initially, when an adsorbent has a lot of porous, its vacant site can adsorb pollutant molecules more than an adsorbent which has a few porous (Zare et al. 2015).

Effect of initial dye concentration on adsorption behavior This is normal because sorption efficiency decreases with increasing initial concentration. After all, more dye concentration has more molecules that can occupy pores of sorbent sooner. So in adsorption, when pollutant concentration is low, the sorbent can work for more quantity of dye wastewater (Wong et al. 2018). As shown in Fig. 6a and d more adsorption capacity occurred when the initial concentration was 10 mg L^{-1}, and in high concentrations such as 250 and 130 mg L^{-1}, low efficiency was observed.

Equilibrium capacity The equilibrium adsorption isotherm of AR18 by WCF/PVA MO NP hydrogel beads under optimum experimental condition (pH = 3; Dosage = 0.55 g L^{-1}; and contact time = 45 min) were investigated as shown in Fig. 6f. Firstly, the elimi-

nation rate of AR18 by WCF/PVA MO NP hydrogel beads increases linearly (first order) with AR 18 concentration, then becomes to mixed order at higher AR18 concentration and leads to reach maximum adsorption capacity (88.65 mg g^{-1}) at the initial concentration of 60 mg L^{-1}, proceeding beyond it at a constant rate (zero-order) (Spagnoli et al. 2017). This means that the presence of a direct correlation of the amount of AR18 adsorbed with AR18 concentration until the reaching maximum adsorption capacity.

Kinetic study The adsorption behaviors of AR18 on the WCF/PVA MO NP hydrogel beads at given time intervals were further investigated by performing kinetic models. From Fig. 7, it is clear that the adsorption capacity increased continuously as the adsorption time increased and finally reached the equilibrium within 45 min, indicating the fast and stable adsorbing performances of AR18 molecules on WCF/PVA MO NP hydrogel beads due to abundant, varied and most stable actives sites on the surface of the adsorbent (Table 1). This occurrence originated from various cross-linking and Lewis's acid sites on the surface of the adsorbent (Liu et al. 2016, Mahvi and Dalvand 2020, Noorimotlagh et al. 2019).

Interestingly, the pseudo-first-order (PFO), pseudo-second-order (PSO), Elovich, and intraparticle diffusion models were carried out to evaluate adsorption kinetics (Ruthven 1984; Vargas et al. 2012):

$$ln\left(q_e - q_t\right) = lnq_e - K_1 t \tag{3}$$

$$\frac{t}{q_t} = \frac{1}{K_2 q_e^2} + \frac{t}{qe} \tag{4}$$

$$q_t = \frac{1}{\beta}\ln\left(a\beta\right) + \frac{1}{\beta}\ln t \tag{5}$$

$$q_t = K_d t^{0.5} \tag{6}$$

where q_e and q_t are the amounts of adsorbed AR18 molecules on the WCF/PVA MO NP hydrogel beads at the optimum condition (mg g^{-1}), t describes the contact time (min), K_1 is the PFO kinetics model constant (min^{-1}), K_2 is the PSO kinetics model constant (g mg^{-1} min^{-1}). α, describe the initial adsorption rate (mg g^{-1} min^{-1}), and β is the desorption constant (g mg^{-1}) represents the chemisorption process rate. Kd (mg g^{-1} $min^{0.5}$) is the rate constant of the intraparticle diffusion model.

According to calculated results (Fig. 7 and Table 2), it is confirmed that the experimental data for describing the adsorption process fitted well with the PSO model due to the higher correlation of coefficient (R^2) and lower Error Analysis (Δq) compared to the PSO, Elovich, and intraparticle models. Chemisorption might be considered as a rate-determining step in the adsorption process (Re). Generally, WCF/PVA MO NP hydrogel beads had a three-dimensional meso/microporous inner structure, facilitating the diffusion of AR18 molecules to the inner structure. In turn, the space of the network of hydrogel beads was increased, resulting in higher/faster adsorption capacity of AR18 by WCF/PVA MO NP hydrogel beads. Incorporating MO NP into hydrogel beads exhibited excellent physical, chemical, and mechanical properties. Due to existing the plentiful external active binding sites that originated from the incorporation of MO NP and the distribution of multiple (and abundant) functional groups such as hydroxyl, carboxyl, epoxide, and aldehyde on the surface derived from applying multiple cross-linking reagents, WCF indicates excellent coordination with MO NP and thus generates excellent hydrogel beads.

Isotherm study

The Langmuir, Freundlich, Temkin, and Dubinin-Radushkevich (D-R) isotherms were performed to evaluate the interaction between AR18 molecules and adsorbent and further investigated the adsorption mechanisms. These models (as brings in Eq. 7 (Langmuir model) (Langmuir 1918), 9 (Freundlich model) (Freundlich 1906), 10(Temkin) (Temkin 1940), and 11(D-R model) (Dubinin 1960)) were successfully fitted into the experimental data:

$$q_e = \frac{q_{max} K_a C_e}{1 + K_a C_e} \tag{7}$$

where q_e is the amount of dye at equilibrium (mg g^{-1}), q_{max} is dye concentration at equilibrium (mg

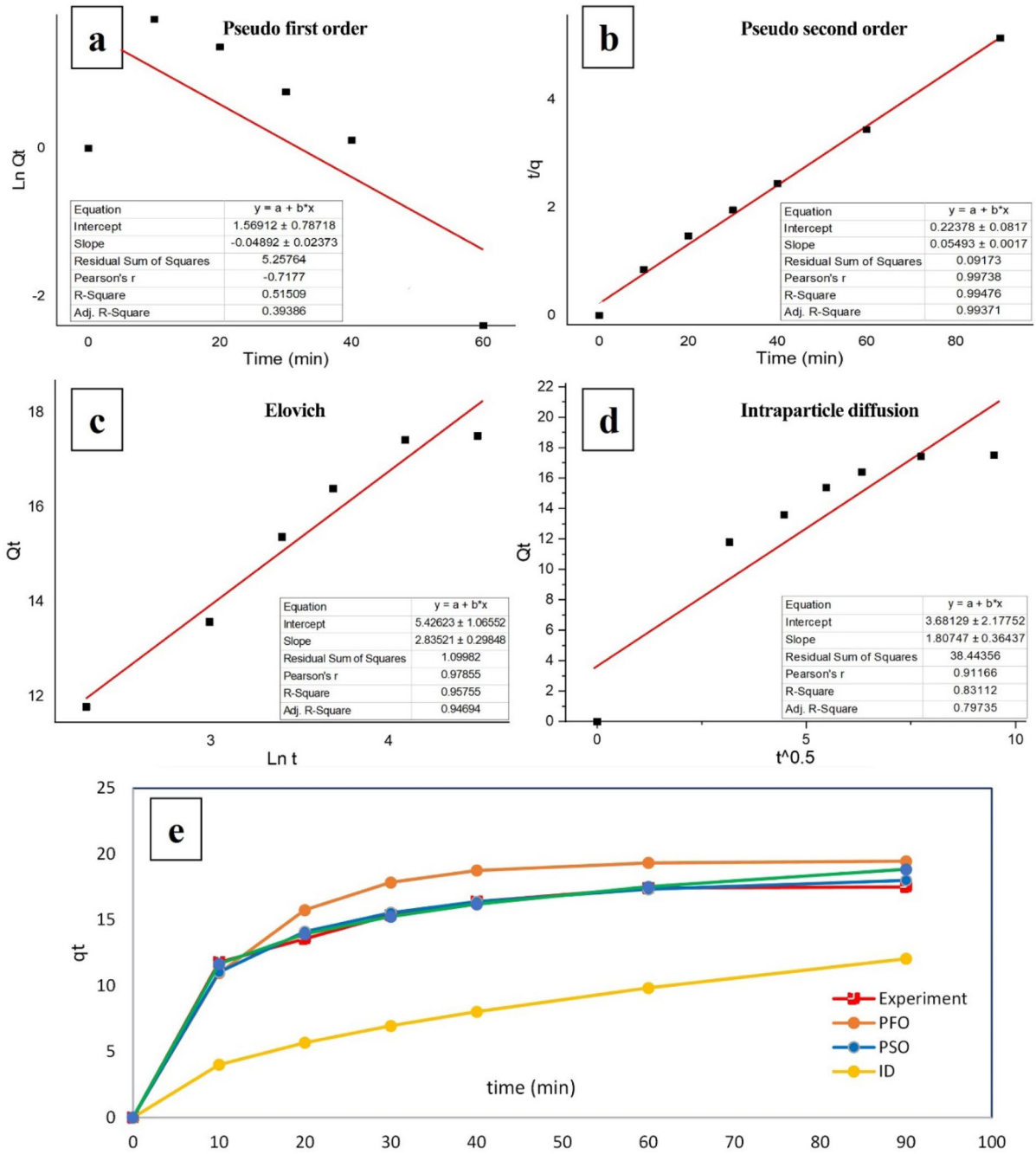

Fig. 7 linear (**a**–**d**) and non-linear (**e**) curves of the kinetic models of AR18 adsorption on the WCF/PVA MO NP hydrogel beads under the optimized condition

g^{-1}), K_a is Langmuir constant (L mg^{-1}), and C_e is Langmuir adsorption capacity (mg L^{-1}). Furthermore, to determine the nature of the adsorption process, a dimensionless constant called equilibrium parameter (R_L) (see Table 2) was used in the following Eq. (8) (Weber and Chakravorti 1974).

Table 1 ANOVA test for CCD modelling and results of process optimization

AR18 ~	DF	SS	MS	F-value	*p* value
Model Statistics					
Model FO	4	9587.4	2396.85	42.0581	2.778e−13
Model PQ	2	1120.0	559.98	9.8261	0.0003778
Residual	37	2108.6	56.99		
Lack of fit	18	1167.1	64.84	1.3086	0.2828385
Pure error	19	941.5	49.55		
R^2	0.8355				
R^2_{adj}	0.8088				
	Coeff. SC	Std. Err	*t* value	*p* value	Sig
Parameters Statistics					
Constant	47.6449	1.4805	32.1816	< 2.2e−16	***
pH	− 26.5734	3.0819	− 8.6224	2.216e−10	***
Dose	11.4481	3.0819	3.7146	0.0006689	***
Time	15.9949	3.0819	5.1899	7.833e−06	***
Initial concentration	− 22.4691	3.0819	− 7.2906	1.166e−08	***
pH*pH	− 16.7895	5.1286	− 3.2737	0.0023065	**
Time*Time	− 13.8779	5.1286	− 2.7060	0.0102391	*
Factor		Value			Unit
Optimization process					
pH		3.00			*
Initial concentration		10			$mg.L^{-1}$
Dose		0.55			$g.L^{-1}$
Time		46			min
Efficiency		87.62			%

$$R_L = \frac{1}{1 + K_a C_0} \tag{8}$$

where C_o is the Initial concentration of AR18 (mg L^{-1}) and K_a is Langmuir adsorption constant (L mg^{-1}) Where the adsorption is irreversible ($R_L = 0$), and linear when ($R_L = 1$), favorable ($0 < R_L < 1$), unfavorable ($R_L > 1$).

$$q_e = K_f C_e^{1/n} \tag{9}$$

where K_f is Freundlich constant (mg g^{-1}) (L $mg^{-1})^{1/n}$ and *n is* adsorption intensity:

$$q_e = \frac{RT}{b_T} \ln\left(K_T C_e\right) \tag{10}$$

where K_T is Temkin constant ($L.mg^{-1}$), R is the universal gas constant (8.314 J mol^{-1} K^{-1}), T is the absolute temperature (K), and b_T is the heat of adsorption (J mol^{-1}).

$$q_e = q_s exp\left(-K_{DR}\epsilon^2\right) \tag{11}$$

It is plain that the experimental data fitted well with the Langmuir model due to the high correlation coefficient, as shown in Fig. 8 and Table 2. It is suggested that the adsorption of AR18 molecules by WCF/PVA MO NP hydrogel beads was monolayer, and the interaction between AR 18 molecules was significantly weak. It is important to note that the calculated Langmuir constant (K_L) was relatively large in comparison to reported values (Czepirski et al. 2000) (0.34 mL mg^{-1}), confirming a strong interaction/binding between AR 18 molecules and WCF/PVA MO NP hydrogel beads. In addition, the favorability of the adsorption process of WCF/PVA MO NP

Table 2 Isotherm, kinetic, and thermodynamic model's parameters for AR18 adsorption on WCF/PVA MO NP hydrogel beads under the optimized condition

Models	Parameters	AR18 Values
Isotherm		
Langmuir	Q_m (g^{-1})	98.65
	K_L (L mg^{-1})	0.34
	R_L	0.01–0.041
	Slope	0.01006 ± 2.95
	Intercept	0.03006
	R^2	0.9948
	Pearsons' r	0.9974
Freundlich	n	2.45
	K_F (L mg^{-1})	27.07
	Slope	0.40916 ± 0.0351
	Intercept	3.29703 ± 0.0765
	R^2	0.95769
	Pearsons' r	0.97862
Temkin	B_l	19.14
	K_T (L mg^{-1})	4.51
	Slope	19.25333 ± 1.5853
	Intercept	28.74936 ± 3.4582
	R^2	0.96091
	Pearsons' r	0.98026
Dubinin and Radushkevich	E (kJ mol^{-1})	1654.67
	D (mol^{-2} kJ^{-2})	0.00000018
	Slope	− 1.8278E−7 ± 4.03999E−8
	Intercept	4.24 ± 0.117
	R^2	0.7733
	Pearsons' r	− 0.8793
Kinetic		
First-order kinetic	k_1(min^{-1})	0.08
	q_e (AR18/g)	19.46
	Slope	− 0.04892 ± 0.02373
	Intercept	1.56912 ± 0.78718
	R^2	0.51509
	Pearsons' r	− 0.7177
Second-order kinetic	k2(g/mg^{-1} min^{-1})	0.00663
	qe (AR18/g)	19.55
	Slope	0.05493 ± 0.0017
	Intercept	0.22378 ± 0.0817
	R^2	0.9947
	Pearsons' r	0.9973

Table 2 (continued)

Models	Parameters	AR18 Values
Intraparticle diffusion	Kdif(g/mg^{-1} min$^{-0.5}$)	1.27
	C	− 8.00
	Slope	1.80747 ± 0.36437
	Intercept	3.68129 ± 2.17752
	R^2	0.8311
	Pearsons' r	0.9116
Elovich	β (g mg^{-1})	3.27
	α (g mg^{-1} min^{-1})	1.09
	Slope	2.83521 ± 0.29848
	Intercept	5.42623 ± 1.06552
	R^2	0.9575
	Pearsons' r	0.97855

Temperature	ln kd	ΔS°(kJ/mol.K)	ΔG°(kJ/mol)	ΔH°(kJ/mol)	qe
Thermodynamic					
283 °K	3.231		− 7.6142		17.37
293 °K	3.3476	0.0604	− 8.1547	− 137.51	17.347
303 °K	3.5186		− 8.8639		17.172
313°K	3.6092		− 9.3922		16.98

hydrogel beads was demonstrated by R_L between 0 and 1 and adsorption intensity (n_F) greater than 1.

The adsorption capacity of the AR 18 molecules by the WCF/PVA MO NP hydrogel beads was lied on the occupancy of active sites over (or inner) the channel surface of WCF/PVA MO NP hydrogel beads by the AR18 molecules through the adsorption process. It has to be ensured that the distribution of functional groups along with their physical stability of them and also the incorporation of MO NP into inner/outer channels of the surface of WCF/PVA MO NP hydrogel beads that both of them serve adsorbed sites actively, generated more opportunity of the interaction of AR 18 molecules and thereby enhancing adsorption of AR 18 on the WCF/PVA MO NP hydrogel beads. It confirmed that the agglomerative and cooperative phenomenon played a main role in AR18 adsorption by multiple cross-linking of WCF/PVA MO NP hydrogel beads.

Thermodynamic study The adsorption process of AR18 on the WCF/PVA MO NP hydrogel beads was further investigated at different temperatures, which is determined based following equations (Bazrafshan et al. 2015):

$$\Delta G^0 = -RTLnK^0 \tag{12}$$

$$\ln\left(\frac{qe}{Ce}\right) = \frac{\Delta S^0}{R} - \frac{\Delta H^0}{RT} \tag{13}$$

$$\Delta G^0 = \Delta H^0 - T\Delta S^0 \tag{14}$$

where ΔG^0 is Gibbs free energy, R is gas constant (8.314 J mol^{-1} K^{-1}), T is the temperature in kelvin degrees, K^0 is the thermodynamic equilibrium constant, C_e is the residual concentration of the absorbed substance in the solution (mg L^{-1}), ΔH^0 is the enthalpy changes and ΔS^0 shows the entropy changes.

As shown in Fig. 9, and Table 2, the Gibbs Free energy (ΔG°) of the adsorption process is negative and increases as reaction temperature increases. It is confirmed that the AR18 adsorption on WCF/PVA MO NP hydrogel beads token place spontaneously and exogenically. On the one hand, the adsorption process by WCF/PVA MO NP hydrogel beads

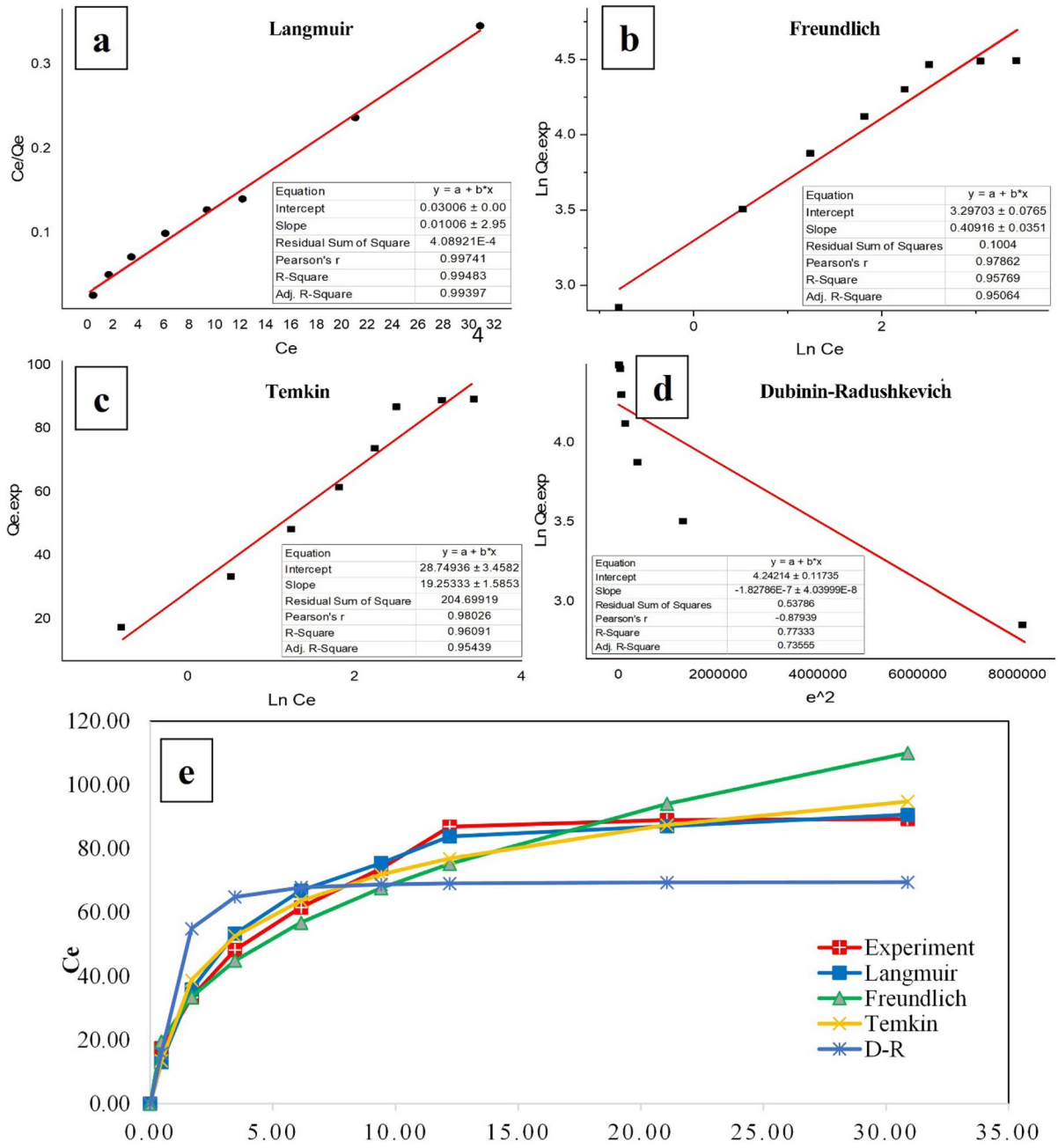

Fig. 8 linear (**a**–**d**) and non-linear (**e**) curves of the isotherm models of AR18 adsorption on the WCF/PVA MO NP hydrogel beads under the optimized condition

will release more energy for the adsorption of AR18 molecules due to multi-active sites and cross-linking functional groups. As presented in Table 2 the ΔG° has a negative value, so the reaction is very spontaneous, and therefore highly favorable, also this negative value confirmed that ΔS° (Entropy) is greater than ΔH° (Enthalpy). Moreover, it is important to note that the adsorption process as temperature increases is more profitable due to not only significantly releasing the H^{+} from functional groups and cross-linking

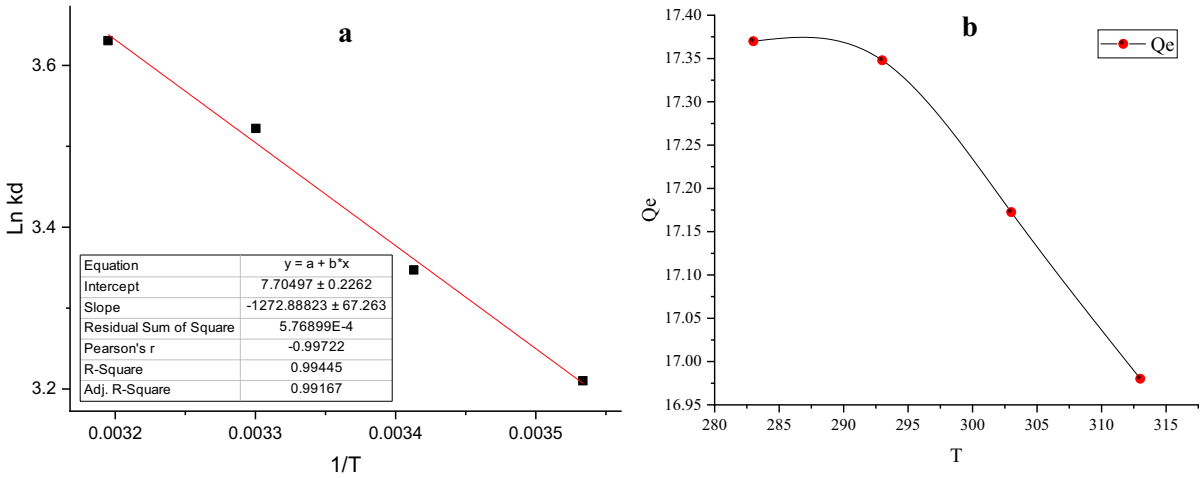

Fig. 9 Linear (**a**) and Non-linear (**b**) curves of the thermodynamic parameters of AR18 adsorption on the WCF/PVA MO NP hydrogel beads under the optimized condition

reagents, particularly the COOH– and OH– but also the cooperative interaction of multi-functionality of functional groups and active site of WCF/PVA MO NP hydrogel beads with AR18 molecules, enhancing their kinetic energy.

The adsorption mechanism of prepared hydrogel beads

It is not usually binding a specific functional group to cellulose when target molecules have not sufficiently reacted with hydroxyl groups. Therefore, we can attach various reactive groups to cellulose hydrogel beads that exhibit great reactivity or selectivity toward the desired molecule. We performed this action on the WCF/MO NP hydrogel beads after extracting cellulose from wastepaper by adding cross-linking agents (or electrophilic reagents), converting WCF/MO NP into desired, various, and multifunctional groups of hydrogel beads. Moreover, introducing MO NP into hydrogel beads could be created additional active sites that have synergetic effects on active metal–acid sites.

The extraction of wastepaper to gain pure cellulose by NaOH and sodium bicarbonate has attached oxirane moieties to the cellulose backbone and leads to activate hydrogel beads. The oxirane groups bound to the WCF/MO NP hydrogel beads might bind with hydroxyl groups or –NH (or –SO3) of the neighboring AR18 molecules, which can lead to adsorbing the AR18.

Another reactive group over WCF/MO NP hydrogel beads is carbonyl moieties confirmed with FTIR spectra (Fig. 3a). it can react with -NH groups of AR18 molecules to form imines (3Re), which could be reduced to amines to raise the chemical stability of linkage between WCF/MO NP hydrogel beads and AR18 molecules.

It is important to note that AR18 molecules could easily penetrate into WCF/MO NP hydrogel beads and build bonds with hydroxyl groups via complexation between the MO NP and the lone pair of electrons of N/O electrostatic interaction or ion exchange between anionic AR18 molecules and protonated groups. Additionally, the WCF/MO NP hydrogel beads can be included reactive species at their active sites, such as acid, bases, and nucleophiles. For example, the H moieties and O^- on the surface of WCF/MO NP hydrogel beads could serve as active acid sites and nucleophilic sites for successfully adsorbed AR18 dyes from an aqueous solution. Interestingly, the sum of –OH groups of PVA and WCF have the chance to be coupled with MO NP as confirmed from FTIR result and created metal–ligand active sites that are available to bind with dyes molecules which finally results in enhanced AR18 sorption. Moreover, the couples –OH groups of PVA and WCF with MO NP before participating it's in the adsorption of AR18 are not created an accessible site to interact

Table 3 Comparison between maximum adsorption capacities for AR18 removal from aqueous solution by variant adsorbents reported in the literature

Adsorbent	Isotherm	Kinetic	qm (AR18/g)	Ref
WCF/PVA MO NP hydrogel beads	Langmuir	PSO	88.65	This study
Cobalt/carbon	Langmuir	PSO	42.5	Han et al. (2018)
Activated charcoal	Freundlich	PSO	10.752	Chaleshtori et al. (2017)
PSAC	Langmuir	PSO	34.247	Saratale et al. (2016)
ACW	Langmuir	PSO	30.3	Heibati et al. (2015b)
ACP	Freundlich	PFO	3.91	Heibati et al. (2015b)
MQAS-WB	Langmuir	PSO	20.61	Zhang et al. (2018)

with water molecules and thereby reducing moisture sorption.

Some comments and suggestions from earlier reported to hydrogel bead recovery

The adsorption capacity of the AR18 dyes by the WCF/PVA MO NP hydrogel beads in this study was remarkably higher than in reported studies, as shown in Table 3. The as-prepared hydrogel beads indicate multi and various functional groups that generated appropriate bonds with dye molecules and WCF/PVA MO NP hydrogel beads, suggesting a promising adsorbent for cleaning wastewater from cationic pollutants.

Figure 10 shows the results after each cycle. The removal efficiency of the first two cycles remains high, which is 95.3% and 92.16%, respectively. After the fifth cycle removal percentage reached 74.36%, which was an excellent efficiency; after the fifth usage of cellulosic adsorbent, the optimum condition was considered. After the sixth cycle, the removal efficiency was lower than 70% and decreased efficiency as the number of cycles increased.

In this study, the WCF/PVA MO NP hydrogel beads were recovered at least six recyclable cycles under hydrochloric acid treatment, as can be seen in Fig. 10. When the adsorption process reached equilibrium, the volume of used acid that needed to be reached a high regenerated adsorption capacity of WCF/PVA MO NP hydrogel beads was exceeded that that major experimental AR18 solution. However, it could be considered as a secondary pollutant for the aqueous environment, no important what type of eluents were carried out for desorption. This condition is become worse for hydrogel beads due to

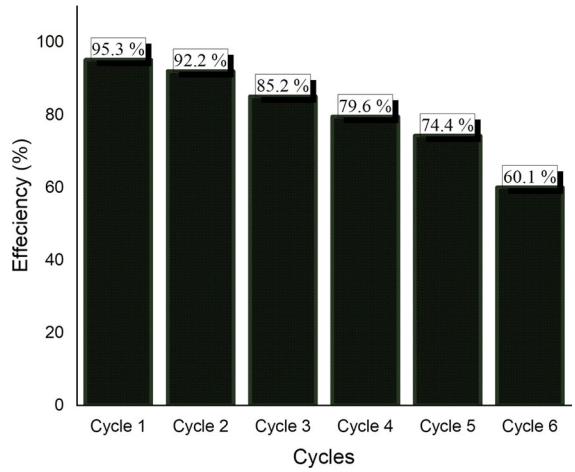

Fig. 10 Reusability of the WCF/PVA MO NP hydrogel beads for AR18 removal

softly and super-hydrophobically properties. Hence, in this study, an aqueous solution of HCl 0.1 N was used to perform the desorption tests and then evaluate the recovered adsorption capacity of the WCF/PVA MO NP hydrogel beads under shaking at 250 rpm for 2 h. many reports widely evaluate the recovery ability of hydrogel adsorbents but neglecting the releasing of eluents into the environment might be adverse effects during desorption experiments (Re4). As prepared and developed, hydrogel beads in this study demonstrated a high adsorption capacity and can be tightly trapped the pollutant in its body to reduce the potential risk to the environment, suggesting that minimizing the potential risk to the environment was more important than that high ability of recovery and regeneration.

Conclusions

The development of novel hydrogel beads with 3D polymer networks that PVA cross-links and then boron and calcium mixed cross-linker agents and MO NP distribution have been successfully prepared. Considering their advantages, such as low cost, non-toxicity, multifarious porous structure, multitudinous active groups from Bronsted and Lewis acid-sites to active metal–acid sites, biocompatibility, strongly mechanical features (which ascribed to inherent good strength of WCF and their interactions with cross-linking agents), and fast equilibrium period of contact reaction time, it is not surprising that these hydrogel beads have demonstrated a rapid and high adsorption capacity and in particular, their good adsorbing potential for AR18 molecules from aqueous solution. Accordingly, the adsorption of AR18 on the surface of hydrogel beads is significantly affected by pH, where ideal adsorption occurs at pH 3. Introducing MO NP to the WCF can enhance the characteristics and/or functionalities of the prepared hydrogel beads and mechanical strength or chemical stability. In addition, MO NP could introduce additional active metal–acid sites and can even enhance the density of functional groups at the interior/or exterior of the hydrogel beads. The experimental data were fitted well with Langmuir and pseudo-second-order models. The spontaneous, exothermic, and chemosorption characteristics of the adsorption process are confirmed based on negative values of ΔG° and fitted experiments with Langmuir isotherm, respectively. In conclusion, the hydrogel beads and their prepared approach used in this study could also serve as a cost-effective, recyclable, recovery capability, and stable polymer for developing advanced adsorbent-based polymer and/or polymer-inorganic composites with promising properties.

Acknowledgments The authors would like to gratefully acknowledge the financial support provided by the Tehran University of Medical Sciences.

Authors contribution MRG: Conceptualization, Methodology, Validation, Writing—original draft, Writing—review and editing. DS: Conceptualization, Methodology, review and editing, Writing—original draft. RN: Methodology, Conceptualization, Visualization, Validation. AHM: Conceptualization, Methodology, review and editing, Writing—original draft, Supervision, Project administration.

Funding Research reported in this publication was supported by Elite Researcher Grant Committee under award number [46988] from Tehran University of Medical Sciences (TUMS), Tehran, Iran.

Data availability All data generated or analyzed during this study are included in this published article.

Declarations

Conflict of interest The authors declare that they have no known competing financial interests or personal relationships that could have appeared to influence the work reported in this paper.

Consent to participate Not applicable.

Consent to publish Not applicable.

Ethical approval IR.TUMS.SPH.REC.1399.014.

References

Abe K, Yano H (2011) Formation of hydrogels from cellulose nanofibers. Carbohydr Polym 85:733–737

Abràmoff MD, Magalhães PJ, Ram SJ (2004) Image Processing with ImageJ. Biophotonics Int 11:36–42

Alibak AH, Khodarahmi M, Fayyazsanavi P, Alizadeh SM, Hadi AJ, Aminzadehsarikhanbeglou E (2022) Simulation the adsorption capacity of polyvinyl alcohol/carboxymethyl cellulose based hydrogels towards methylene blue in aqueous solutions using cascade correlation neural network (CCNN) technique. J Clean Prod 337:130509

Alizadeh-Sani M, Tavassoli M, McClements DJ, Hamishehkar H (2021) Multifunctional halochromic packaging materials: Saffron petal anthocyanin loaded-chitosan nanofiber/methyl cellulose matrices. Food Hydrocolloids 111:106237

Araki J (2021) Dye adsorption revisited: application of the cationic dye adsorption method for the quantitative determination of the acidic surface groups of nanocellulose materials. Cellulose 28:7707–7715

Arora C, Soni S, Sahu S, Mittal J, Kumar P, Bajpai P (2019) Iron based metal organic framework for efficient removal of methylene blue dye from industrial waste. J Mol Liq 284:343–352

Ashrafi SD, Rezaei S, Forootanfar H, Mahvi AH, Faramarzi MA (2013) The enzymatic decolorization and detoxification of synthetic dyes by the laccase from a soil-isolated ascomycete, Paraconiothyrium variabile. Int Biodeterior Biodegrad 85:173–181

Athar T (2013) Synthesis and characterization of strontium oxide nanoparticles via wet process. Mater Focus 2:450–453

Atykyan N, Revin V, Shutova V (2020) Raman and FT-IR Spectroscopy investigation the cellulose structural differences from bacteria Gluconacetobacter sucrofermentans

during the different regimes of cultivation on a molasses media. AMB Express 10:1–11
Azari A, Nabizadeh R, Nasseri S, Mahvi AH, Mesdaghinia AR (2020) Comprehensive systematic review and meta-analysis of dyes adsorption by carbon-based adsorbent materials: Classification and analysis of last decade studies. Chemosphere 250:126238
Bazrafshan E, Alipour MR, Mahvi AH (2016) Textile wastewater treatment by application of combined chemical coagulation, electrocoagulation, and adsorption processes. Desalin Water Treat 57:9203–9215
Bazrafshan E, Mostafapour FK, Hosseini AR, Raksh Khorshid A, Mahvi AH (2013) Decolorisation of reactive red 120 dye by using single-walled carbon nanotubes in aqueous solutions. J Chem 2013
Beh JH, Lim TH, Lew JH, Lai JC (2020) Cellulose nanofibril-based aerogel derived from sago pith waste and its application on methylene blue removal. Int J Biol Macromol 1:836–845
Chaleshtori AN, Meghadddam FM, Sadeghi M, Rahimi R, Hemati S, Ahmadi A (2017) Removal of Acid Red 18 (Azo-Dye) from aqueous solution by adsorption onto activated charcoal prepared from almond shell. J Environ Sci Manag 20:9–16
Chaugule AA, Mane VS, Bandal HA, Kim H, Kumbhar AS (2019) Ionic liquid-derived Co3O4-N/S-doped carbon catalysts for the enhanced water oxidation. ACS Sustain Chem Eng 7:14889–14898
Chen P, Liu X, Jin R, Nie W, Zhou Y (2017) Dye adsorption and photo-induced recycling of hydroxypropyl cellulose/molybdenum disulfide composite hydrogels. Carbohydr Polym 167:36–43
Chen X, Chen C, Zhu J (2019) Facile preparation of cellulose–attapulgite nanocomposite hydrogel for dye adsorption. Iran Polym J 28:347–359
Czepirski L, Balys MR, Komorowska-Czepirska E (2000) Some generalization of Langmuir adsorption isotherm. Internet J Chem 3:1099–8292
Dai H, Huang Y, Huang H (2018) Eco-friendly polyvinyl alcohol/carboxymethyl cellulose hydrogels reinforced with graphene oxide and bentonite for enhanced adsorption of methylene blue. Carbohydr Polym 185:1–11
Dalvand A, Nabizadeh R, Ganjali MR, Khoobi M, Nazmara S, Mahvi AH (2016) Modeling of Reactive Blue 19 azo dye removal from colored textile wastewater using L-arginine-functionalized Fe3O4 nanoparticles: optimization, reusability, kinetic and equilibrium studies. J Magn Magn Mater 404:179–189
Dehghani MH, Sanaei D, Ali I, Bhatnagar A (2016) Removal of chromium (VI) from aqueous solution using treated waste newspaper as a low-cost adsorbent: kinetic modeling and isotherm studies. J Mol Liq 215:671–679
Dubinin M (1960) The potential theory of adsorption of gases and vapors for adsorbents with energetically nonuniform surfaces. Chem Rev 60:235–241
Ebadi A, Mohammadzadeh JSS, Khudiev A (2009) What is the correct form of BET isotherm for modeling liquid phase adsorption? Adsorption 15:65–73
Edzwald J, Association AWW (2011) Water quality & treatment: a handbook on drinking water. McGraw-Hill Education, New York
French AD (2014) Idealized powder diffraction patterns for cellulose polymorphs. Cellulose 21:885–896
French AD (2017) Glucose, not cellobiose, is the repeating unit of cellulose and why that is important. Cellulose 24:4605–4609
Freundlich H (1906) Over the adsorption in solution. J Phys Chem 57:1100–1107
Gholami-Borujeni F, Mahvi AH, Naseri S, Faramarzi MA, Nabizadeh R, Alimohammadi M (2011a) Application of immobilized horseradish peroxidase for removal and detoxification of azo dye from aqueous solution. Res J Chem Environ 15:217–222
Gholami-Borujeni F, Mahvi AH, Nasseri S, Faramarzi MA, Nabizadeh R, Alimohammadi M (2011b) Enzymatic treatment and detoxification of acid orange 7 from textile wastewater. Appl Biochem Biotechnol 165:1274–1284
Hamidi F, Dehghani MH, Kasraee M, Salari M, Shiri L, Mahvi AH (2022) Acid red 18 removal from aqueous solution by nanocrystalline granular ferric hydroxide (GFH); Optimization by response surface methodology & genetic-algorithm. Sci Rep 12:1–15
Han T-T, Bai H-L, Liu Y-Y, Ma J-F (2018) Synthesis of nanoporous cobalt/carbon materials by a carbonized zeolitic imidazolate framework-9 and adsorption of dyes. New J Chem 42:717–724
Hashemkhani M, Rezvani Ghalhari M, Bashardoust P, Hosseini SS, Mesdaghinia A, Mahvi AH (2022) Fluoride removal from aqueous solution via environmentally friendly adsorbent derived from seashell. Sci Rep 12:9655
Heibati B, Rodriguez-Couto S, Al-Ghouti MA, Asif M, Tyagi I, Agarwal S, Gupta VK (2015a) Kinetics and thermodynamics of enhanced adsorption of the dye AR 18 using activated carbons prepared from walnut and poplar woods. J Mol Liq 208:99–105
Jiang M, Niu N, Chen L (2022) A template synthesized strategy on bentonite-doped lignin hydrogel spheres for organic dyes removal. Sep Purif Technol 285:120376
Jin L, Li W, Xu Q, Sun Q (2015) Amino-functionalized nanocrystalline cellulose as an adsorbent for anionic dyes. Cellulose 22:2443–2456
Joshi G, Naithani S, Varshney V, Bisht SS, Rana V, Gupta P (2015) Synthesis and characterization of carboxymethyl cellulose from office waste paper: a greener approach towards waste management. J Waste Manag 38:33–40
Kord Mostafapour F, Zolghadr R, Khodadadi Saloot M, Mahvi AH, Balarak D, Safari E (2022) Removal of Acid blue 113 from aqueous medium using a novel magnetic adsorbent derived from activated carbon fiber. Int J Environ Anal Chem 102:1–16
Kumar KY, Muralidhara H, Nayaka YA, Balasubramanyam J, Hanumanthappa H (2013) Low-cost synthesis of metal oxide nanoparticles and their application in adsorption of commercial dye and heavy metal ion in aqueous solution. Powder Technol 246:125–136
Langmuir I (1918) The adsorption of gases on plane surfaces of glass, mica and platinum. J Am Chem Soc 40:1361–1403
Li J, Yang Z-l, Ding T, Song Y-J, Li H-C, Li D-q, Chen S, Xu F (2022a) The role of surface functional groups of pectin and pectin-based materials on the adsorption of heavy metal ions and dyes. Carbohydr Polym 276:118789

Li K, Li X, Wang D, Yang B, Liu Y, Wang H, Shen Y (2022b) Preparation of cross-linking PVA copolymer modified by DAAM/ADH and application in paper surface sizing. Cellulose 29:6845–6863

Lin F, You Y, Yang X, Jiang X, Lu Q, Wang T, Huang B, Lu B (2017) Microwave-assisted facile synthesis of TEMPO-oxidized cellulose beads with high adsorption capacity for organic dyes. Cellulose 24:5025–5040

Liu Z, Zhang F, Liu T, Peng N, Gai C (2016) Removal of azo dye by a highly graphitized and heteroatom doped carbon derived from fish waste: adsorption equilibrium and kinetics. J Environ Manage 182:446–454

Lyu W, Li J, Zheng L, Liu H, Chen J, Zhang W, Liao Y (2021) Fabrication of 3D compressible polyaniline/cellulose nanofiber aerogel for highly efficient removal of organic pollutants and its environmental-friendly regeneration by peroxydisulfate process. Chem Eng J 414:128931

Mahvi AH, Dalvand A (2020) Kinetic and equilibrium studies on the adsorption of Direct Red 23 dye from aqueous solution using montmorillonite nanoclay. Water Qual Res J 55:132–144

Maiti M, Sarkar M, Maiti S, Malik MA, Xu S (2020) Modification of geopolymer with size controlled TiO2 nanoparticle for enhanced durability and catalytic dye degradation under UV light. J Clean Prod 255:120183

Mirzadeh S-S, Khezri S-M, Rezaei S, Forootanfar H, Mahvi AH, Faramarzi MA (2014) Decolorization of two synthetic dyes using the purified laccase of Paraconiothyrium variabile immobilized on porous silica beads. J Environ Health Sci Eng 12:1–9

Mondal AK, Xu D, Wu S, Zou Q, Lin W, Huang F, Ni Y (2022) High lignin containing hydrogels with excellent conducting, self-healing, antibacterial, dye adsorbing, sensing, moist-induced power generating and supercapacitance properties. Int J Biol Macromol 207:48–61

Noorimotlagh Z, Mirzaee SA, Martinez SS, Alavi S, Ahmadi M, Jaafarzadeh N (2019) Adsorption of textile dye in activated carbons prepared from DVD and CD wastes modified with multi-wall carbon nanotubes: equilibrium isotherms, kinetics and thermodynamic study. Chem Eng Res Des 141:290–301

Peng N, Hu D, Zeng J, Li Y, Liang L, Chang C (2016) Superabsorbent cellulose–clay nanocomposite hydrogels for highly efficient removal of dye in water. ACS Sustain Chem Eng 4:7217–7224

Rahmani M, Kaykhaii M, Sasani M (2018) Application of Taguchi L16 design method for comparative study of ability of 3A zeolite in removal of Rhodamine B and Malachite green from environmental water samples. Spectrochim Acta A Mol Biomol Spectrosc 188:164–169

Rejek M, Grzechulska-Damszel J, Schmidt B (2021) Synthesis, characterization, and evaluation of degussa P25/chitosan composites for the photocatalytic removal of sertraline and acid Red 18 from water. J Polym Environ 29: 1–8

Ruthven DM (1984) Principles of adsorption and adsorption processes. John Wiley & Sons, Hoboken

Sani MA, Maleki M, Eghbaljoo-Gharehgheshlaghi H, Khezerlou A, Mohammadian E, Liu Q, Jafari SM (2022) Titanium dioxide nanoparticles as multifunctional surface-active materials for smart/active nanocomposite packaging films. Adv Coll Interface Sci 300:102593

Saratale RG, Sivapathan SS, Jung WJ, Kim HY, Saratale GD, Kim DS (2016) Preparation of activated carbons from peach stone by H4P2O7 activation and its application for the removal of Acid Red 18 and dye containing wastewater. J Environ Sci Health A 51:164–177

Shadkam R, Naderi M, Ghazitabar A, Akbari S (2021) Adsorption performance of reduced graphene-oxide/cellulose nano-crystal hybrid aerogels reinforced with waste-paper extracted cellulose-fibers for the removal of toluene pollution. Mater Today Commun 28:102610

Shirmardi M, Mesdaghinia A, Mahvi AH, Nasseri S, Nabizadeh R (2012) Kinetics and equilibrium studies on adsorption of acid red 18 (Azo-Dye) using multiwall carbon nanotubes (MWCNTs) from aqueous solution. E-J Chem 9:541909

Sillanpää M, Mahvi AH, Balarak D, Khatibi AD (2021) Adsorption of Acid orange 7 dyes from aqueous solution using Polypyrrole/nanosilica composite: experimental and modelling. Int J Environ Anal Chem 101: 1–18

Siripongpreda T, Somchob B, Rodthongkum N, Hoven VP (2021) Bacterial cellulose-based re-swellable hydrogel: facile preparation and its potential application as colorimetric sensor of sweat pH and glucose. Carbohydr Polym 256:117506

Sotomayor FJ, Cychosz KA, Thommes M (2018) Characterization of micro/mesoporous materials by physisorption: concepts and case studies. Acc Mater Surf Res 3:34–50

Spagnoli AA, Giannakoudakis DA, Bashkova S (2017) Adsorption of methylene blue on cashew nut shell based carbons activated with zinc chloride: the role of surface and structural parameters. J Mol Liq 229:465–471

Temkin M (1940) Kinetics of ammonia synthesis on promoted iron catalysts. Acta Physiochim URSS 12:327–356

Thombare N, Mahto A, Singh D, Chowdhury AR, Ansari MF (2023) Comparative FTIR characterization of various natural gums: a criterion for their identification. J Polym Environ 31: 1–9

Vargas AM, Cazetta AL, Martins AC, Moraes JC, Garcia EE, Gauze GF, Costa WF, Almeida VC (2012) Kinetic and equilibrium studies: adsorption of food dyes Acid Yellow 6, Acid Yellow 23, and Acid Red 18 on activated carbon from flamboyant pods. Chem Eng J 181:243–250

Wang C-H, Hsu H-C, Hu J-H (2014) High-energy asymmetric supercapacitor based on petal-shaped MnO_2 nanosheet and carbon nanotube-embedded polyacrylonitrile-based carbon nanofiber working at 2 V in aqueous neutral electrolyte. J Power Sources 249:1–8

Wang Z, Qiu T, Guo L, Ye J, He L, Li X (2019) The building of molecularly imprinted single hole hollow particles: a miniemulsion polymerization approach. Chem Eng J 357:348–357

Wang W, Hu J, Zhang R, Yan C, Cui L, Zhu J (2021) A pH-responsive carboxymethyl cellulose/chitosan hydrogel for adsorption and desorption of anionic and cationic dyes. Cellulose 28:897–909

Wang X, Fan X, Xie H, Li X, Hao C (2022) Polyacrylic acid/carboxymethyl cellulose/activated carbon composite hydrogel for removal of heavy metal ion and cationic dye. Cellulose 29:483–501

Wang X, Deng B, Yu L, Cui E, Xiang Z, Lu W (2020) Degradation of azo dyes Congo red by MnBi alloy powders:

performance, kinetics and mechanism. Mater Chem Phys 251: 123096

Weber TW, Chakravorti RK (1974) Pore and solid diffusion models for fixed-bed adsorbers. AlChE J 20:228–238

Wong S, Yac'cob NAN, Ngadi N, Hassan O, Inuwa IM (2018) From pollutant to solution of wastewater pollution: synthesis of activated carbon from textile sludge for dye adsorption. Chin J Chem Eng 26:870–878

Wu S, Sun A, Zhai F, Wang J, Xu W, Zhang Q, Volinsky AA (2011) Fe_3O_4 magnetic nanoparticles synthesis from tailings by ultrasonic chemical co-precipitation. Mater Lett 65:1882–1884

Xie Y, Guo F, Mao J, Huang J, Chen Z, Jiang Y, Lai Y (2021) Freestanding MoS_2@carbonized cellulose aerogel derived from waste cotton for sustainable and highly efficient particulate matter capturing. Sep Purif Technol 254:117571

Zare K, Sadegh H, Shahryari-Ghoshekandi R, Maazinejad B, Ali V, Tyagi I, Agarwal S, Gupta VK (2015) Enhanced removal of toxic Congo red dye using multi walled carbon nanotubes: kinetic, equilibrium studies and its comparison with other adsorbents. J Mol Liq 212:266–271

Zhang W-X, Lai L, Mei P, Li Y, Li Y-H, Liu Y (2018) Enhanced removal efficiency of acid red 18 from aqueous solution using wheat bran modified by multiple quaternary ammonium salts. Chem Phys Lett 710:193–201